Available online at www.sciencedirect.com
SCIENCE DIRECT®
Journal of Hydrology 292 (2004) 48–58
Journal of Hydrology
www.elsevier.com/locate/jhydrol

Predicting locations sensitive to flash flooding in an arid environment

Giles M. Foody[a,*], Eman M. Ghoneim[b], Nigel W. Arnell[a]

[a]School of Geography, University of Southampton, Highfield, Southampton SO17 1BJ, UK
[b]Centre for Remote Sensing, University of Boston, 725 Commonwealth Avenue, Boston, MA 02215, USA

Received 5 September 2002; revised 2 December 2003; accepted 29 December 2003

Abstract

Flash floods are a common, but poorly understood feature of arid environments. Much of the uncertainty associated with flash flooding events is associated with a lack of accurate environmental data. In addition to limiting the understanding of hydrological processes, this situation handicaps human use and development in such regions, necessitating the use of modelling approaches for environmental prediction. Here, a hydrological model driven mainly by information on land cover distribution (derived by satellite remote sensing) and soil properties (derived from field measurement) was used to predict sites at risk from large peak flows associated with flash flooding in a wadi located in the Eastern Desert of Egypt. The land cover map was derived from a maximum likelihood classification of a Landsat TM image and had an estimated accuracy of 89.5%. The soils of the classes depicted in this map differed markedly in terms of texture and permeability, with the field based estimates of infiltration capacity ranging from 0.07 cm h^{-1} for desert pavement through 14.01 cm h^{-1} for unconsolidated wadi bed deposits. Using the derived information within the hydrological modelling system, the discharge from the wadi and its sub-basins was predicted for an assumed severe storm scenario. The outputs of the model indicated two locations within the wadi where a very large peak discharge (>115 m^3 s^{-1}) could be expected. These sites corresponded to those that suffered flood damage in a recent storm event. The results indicate the potential to drive an integrated hydrological model from limited data to derive important and useful hydrological information in a region where data are scarce.

Keywords: Flash flood; Remote sensing; Hydrologic model; Land cover

1. Introduction

Extreme events often exert a disproportionately large effect on the environment, far larger than that associated with the more commonplace typical events, and are those most associated with hazards to humans. The extremes of rainfall, for example, result in a variety of hazardous phenomena ranging from intense drought through to mega- and super-flooding events (Oba, 2001; Herschy, 2002) and associated consequential problems. For example, extremely large rainfall events are linked to life threatening floods, are a major source of erosion and their discharge can be substantial, comparable to the volume of water moved by ocean currents

* Corresponding author. Fax: +44-23-80593295.
E-mail address: g.m.foody@soton.ac.uk (G.M. Foody).

0022-1694/$ - see front matter © 2004 Elsevier B.V. All rights reserved.
doi:10.1016/j.jhydrol.2003.12.045

(Baker et al., 1993; Douglas et al., 1999; Chlebek and Jarabac, 2002; Mimikou et al., 2002). In arid regions, flooding represents a major hazard to human health and well-being as well as to the infrastructure of the societies dwelling in such regions. In such environments, a major concern is flash flooding, events that may develop within a very short period of time.

Flash floods are a major threat to human life and infrastructures. Unfortunately, there is often a lack of data on key hydrological processes in arid areas (Gheith and Sultan, 2002). This limits the ability to understand the flooding process and use this knowledge to minimize its threat to human health and well-being. The lack of understanding sometimes compounds problems of flooding, with settlements, roads and other structures inappropriately located and designed relative to the flood risk. The ability to predict sites most prone to flooding would help mitigate against future damage and substantially aid regional development. It would, for example, help direct the planning of drainage constructions such as ditches and culverts along roads to minimise damage and limit flood impacts on the transport system. The prediction of sites prone to flooding and planning of damage minimisation activities cannot be done without spatial information on key hydrological properties of the region.

Sometimes, the required information on regional hydrological properties can be derived from satellite remote sensing (Engman and Gurney, 1991; Foody, 2004). For example, some important hydrological variables, such as evapotranspiration, are, or are strongly correlated with, the basic state variables that control the remotely sensed response of a surface and so can be estimated directly from remotely sensed data. This estimation is, however, difficult and often limited by technical problems such as those associated with the accurate radiometric calibration of the remotely sensed imagery. More commonly, therefore, remotely sensed imagery is used to estimate key hydrological variables indirectly. Frequently, land cover is used as an intermediary between the remotely sensed imagery and desired hydrological variables. Land cover has a strong influence on key hydrological variables such as infiltration, interception and evaporation and typically is the dominant variable determining the remotely sensed response of a site. Consequently, land cover maps derived from remotely sensed data have often been used to estimate a range of hydrological variables for the parameterisation of hydrological models (Hoshi et al., 1989; Sharma and Singh, 1992; Storck et al., 1998; Su, 2000). These models may be used to predict the response of a site to a precipitation event. In particular, the models may be used to predict the storm hydrograph that may help in identifying locations sensitive to flood hazards.

Precipitation events in arid areas are highly variable in space and time (Graef and Haigis, 2001; Gheith and Sultan, 2002). Commonly, desert storms are highly localised, with only part of a catchment receiving rain and contributing directly to surface run-off along wadis. Together with the variation in the nature of the precipitation event, notably its intensity and duration, the variability in the occurrence of precipitation events complicates the understanding of the response of a catchment to rainfall, particularly as there are so few measurements made in the field. In the absence of detailed field measurements, the most appropriate method for predicting the sites prone to flash flooding is to use a spatially distributed hydrological model. Such a model, based on the current understanding of run-off generation and flow, integrated with complete spatial coverage of hydrologically useful properties derived indirectly through a land cover classification of satellite remotely sensed data may be used to predict the shape and magnitude of flood hydrographs. Traditionally, in flooding studies, attention has focused on the variables such as the hydrograph's peak discharge (Papp, 2002). The aim of this article is to evaluate the potential of a modelling based approach for the prediction of sites sensitive to flood hazards in a data-limited arid region using limited field data together with land cover information derived from satellite remote sensor data. Throughout, attention is focused on the relative magnitude of predicted peak discharges as an indicator of flood risk.

2. Test site

The study focused on the wadi El-Alam in Eastern Egypt (Fig. 1). This is fairly typical of watersheds in arid regions, especially of the mountain wadis of the Eastern Desert and Sinai

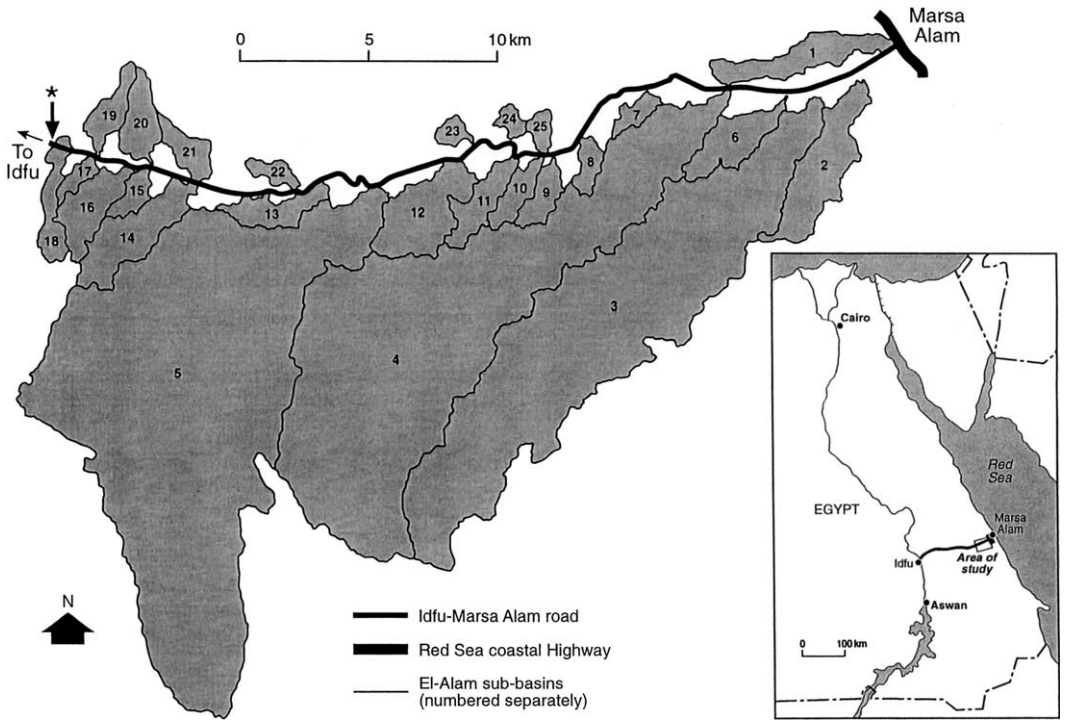

Fig. 1. Location of the test site and the basins included in the analyses. The symbol * represents the edge of the catchment from which distance along the road are measured.

Peninsular, with rugged terrain, little vegetation and relatively shallow soils. Furthermore, like other wadis in the region, settlements have developed at or near the outlet and roads traverse the wadi basin. In the instance of wadi El-Alam, a major human settlement, Marsa-Alam, is located at the basin's outlet and this is connected to the town of Idfu by a road that runs through the wadi. Consequently, both the urban area of Marsa-Alam and road inland to Idfu are potentially vulnerable to flooding and associated damage. Particular attention here is focused on the Idfu-Marsa-Alam road that has previously been damaged by flash floods (El-Etr and Ashmawy, 1993). In particular, the 36 km section of the road that runs through the wadi and which has mainly been constructed on the floor of the drainage course, crossing the alluvial fans of numerous sub-basins, was the prime focus of attention (Fig. 2).

Although, located within an arid-hyperarid region, with an average annual rainfall of 13 mm, the region does experience intense rainfall events infrequently. These rainfall events are often associated with severe local convective thunderstorms (Zeller, 1990; Greenbaum et al., 1998) and although typically having a short duration, less than 4 h, may have an intensity of >30 mm h^{-1} (Sabol and Stevens, 1990). For example, Zeller (1990) reports on a rainstorm in Arizona in which 130 mm of rain fell within 2 h and Gheith and Sultan (2002) report on storms producing of up to 60 mm of rainfall at locations near the current test site. Such storms can rapidly generate flash floods, the size of which varies as a function of both the rainfall event and the characteristics of the basin. Understanding flash flooding at the site and predicting sites vulnerable to flood damage is, however, hampered by a lack of data. The basin itself is ungauged and there is very little meteorological data for the site; the nearest meteorological station is some 70 km away. Furthermore, there are considerable uncertainties associated with the composition of the site. In particular, the hydrological properties

Fig. 2. Oblique view of the Idfu-Marsa-Alam road crossing through the wadi El-Alam. Note the road crossing the relatively flat wadi bed and topographic shadowing.

of the land cover, which is not mapped accurately, is unknown, limiting the ability to drive predictive models.

3. Data and methods

In the absence of detailed data, especially on rainfall and ground surface properties for the site, the only feasible means of predicting sites sensitive to flooding was to adopt a modelling approach supported by acquisition of data on land cover and associated hydrological variables. Given the spatial variability in rainfall and basin hydrological properties, a spatially distributed rather than lumped model was required. Here, the hydrologic modelling system (HMS), using Muskingum flow routing (Chow et al., 1988), developed by the Hydrologic Engineering Center of the US Army Corps of Engineers, was selected. The HMS was used to model the rainfall-runoff processes of the basin and predict the hydrograph at locations within it. Model parameters, outlined below, were determined with the CRWR-PrePro system (Olivera and Maidment, 1999). CRWR-PrePro extracts topographic, topologic and hydrological information from digital elevation data. The latter were derived by manually digitising contours from 1:50,000 topographic maps of the site.

The HMS model is described in detail by Peters (1998). With this model, the basin is viewed as a series of hydrological elements linked in a series. The model routes water from one element to another until some terminal point is reached. It uses descriptions of the hydrological elements of the basin, such as its river reaches, junctions, reservoirs, sources and sinks as well as sub-basins, together with routing parameters to model the movement of water over the site. Water losses due to infiltration were computed using the Soil Conservation Service curve number method. This method estimates runoff as a function of the cumulative precipitation, antecedent moisture, soil and land use conditions. The curve number is a function of soil and land cover conditions, which may be estimated using published tables (SCS, 1985) from information on land cover, soil type and antecedent moisture conditions. The estimation of the curve number, therefore, required information on these three variables. For this test site, in an arid environment, it seems reasonable to assume dry antecedent moisture conditions (Gheith and Sultan, 2002). Information on the remaining two variables, soil and land cover, was derived from fieldwork and through satellite remote sensing.

The land cover information required for the hydrological modelling were derived with the aid of a supervised digital image classification (Tso and Mather, 2001) of the Landsat TM imagery of the site. This analysis aimed to derive a thematic classification from the imagery in which the land cover classes mapped differed in terms of their hydrological

properties. From field observation, the site comprised a small number of land covers, namely bedrock outcrops, desert pavement, and consolidated and unconsolidated wadi bed deposits. The physical differences between these surfaces give rise to differences in their permeability and thus their infiltration and run-off properties. The spatial distribution of these different classes within a catchment would, therefore, impact considerably on the catchment's response to a rainfall event. Consequently, a map of these classes was derived from the Landsat TM data and a field study undertaken to measure key properties.

The TM data used were acquired in March 1988 and had a spatial resolution of 30 m in the non-thermal wavebands; the data acquired in TM band 6 (thermal infrared) were not used because of their coarse, 120 m, spatial resolution. Landsat TM data have been widely used for mapping land cover in a range of environments, including arid regions (Langley et al., 2001; Gheith and Sultan, 2002). These data were rigorously pre-processed using standard techniques prior to the classification (Mather, 1999). This pre-processing aimed to ensure that the variation in remotely sensed spectral response observed was, as far as possible, a function only of land surface properties, notably soil and land cover, so that hydrologically useful thematic classification could be derived. The pre-processing involved geometric, atmospheric, radiometric and topographic correction of the remotely sensed data.

The geometric correction was achieved using a transformation equation derived from 14 ground control points dispersed over the test site. Nearest neighbour resampling was used to maintain the data's statistical properties. The estimated root mean square error of the geometric transformation was 0.7 pixel. The data were radiometrically corrected using published gain and offset coefficients for the sensor to convert the image digital numbers to radiance. In the absence of detailed data on atmospheric conditions, a simple but effective image-based method, the refined dark object subtract method proposed by Chavez (1996), was used to reduce atmospheric effects in the data (Song et al., 2001). Finally, a topographic correction was made to compensate for the effects of variable surface illumination due to topographic variation. The method used was that suggested by Ekstrand (1996) with the Minnaert constant used to reduce the potential for over-correction for topographic effects. Although, there are problems associated with use of Minnaert based topographic corrections (Bishop and Colby, 2002), the Minnaert constant was estimated globally over the site using an empirical regression approach (Colby and Keating, 1998). The resulting topographic correction reduced the effects of variations in terrain surface orientation and topographic shading (Fig. 2) on the remotely sensed response (Fig. 3). The final pre-classification step was a feature selection to reduce the size of the data set (Mather, 1999). Commonly, remotely sensed imagery contains a high degree of redundancy, with

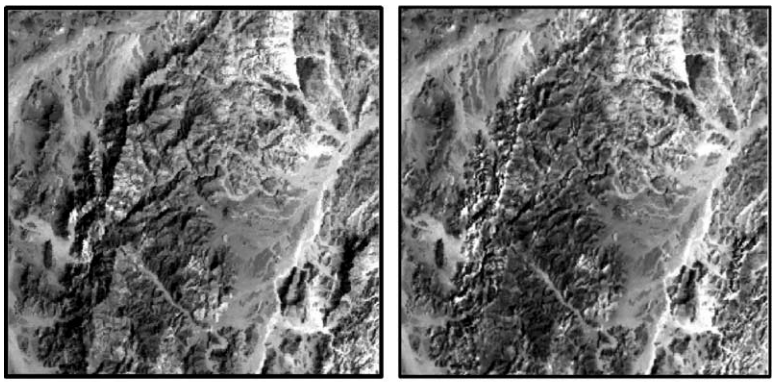

(a) (b)

Fig. 3. Landsat TM image, band 4 (near-infrared), of the test site (a) before and (b) after topographic correction.

the dimensionality of the data set smaller than the number of wavebands. Since redundant data can degrade classification performance and accuracy, a feature selection was undertaken to exclude unnecessary data. On the basis of the degree of inter-waveband correlation observed, the data acquired in Landsat TM bands 3–5 and 7 only were selected for use.

The land cover map was derived using a supervised image classification (Tso and Mather, 2001). From both field observation and visual interpretation of the remotely sensed imagery, it was, however, apparent that the bedrock outcrops comprised two spectrally separate classes, with basement (igneous and metamorphic) rocks dominating the catchment area and a small region of sedimentary rocks located near the Red Sea coast. To limit the potential for inter-class confusion and so facilitate accurate mapping, the bedrock class was divided into its two component classes for the production of the land cover map from the remotely sensed imagery. These classes were, however, amalgamated post-classification to represent the bedrock class as they have the same hydrological properties in the model. For each of the five thematic classes to be mapped classes (including sedimentary and basement rocks), five training sites were identified for each class and used to derive training statistics for a conventional maximum likelihood classification. This approach allocates each pixel in the image to the class with which it has the greatest posterior probability of membership (Tso and Mather, 2001). The output of the latter was a thematic map depicting the spatial distribution of the five selected land cover classes over the basin (Fig. 4).

The accuracy of the derived land cover map was assessed from a random sample of 229 pixels. For each of these pixels the actual land cover class was derived from 1:40,000 scale aerial photographs acquired in 1989; the nature of the environment dictates that (aside from short lived vegetal changes) the land surface cover is highly intransient and so the ~1 year difference in the date of aerial photograph and Landsat TM data acquisition was unimportant.

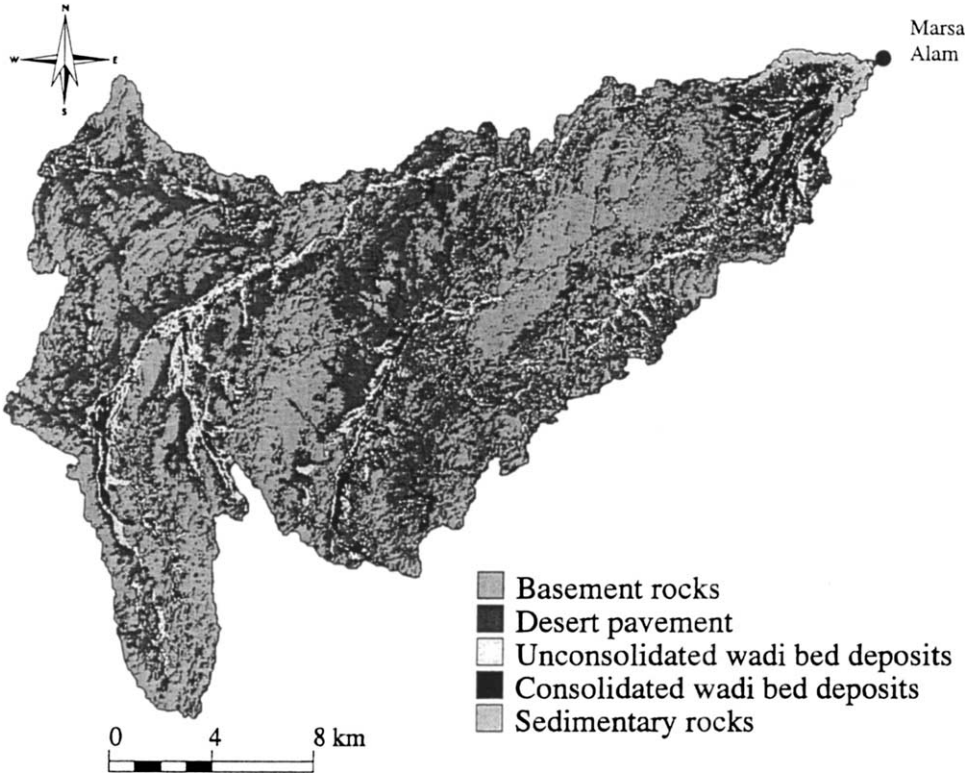

Fig. 4. Land cover classification derived from a supervised maximum likelihood classification of the Landsat TM data.

Settlements and roads, manually digitised from 1:50,000 scale topographic maps of the site, were added to the land cover map derived from the classification of the Landsat TM imagery. The resulting seven class map was used in the estimation of curve numbers in the HMS based analyses.

The field surveys aimed to evaluate the textural and infiltration properties of the non-rock classes. This information was required for the determination of soil groups, a necessary requirement for the specification of curve numbers in the model (SCS, 1985). Fieldwork undertaken in February 1999 and January 2001 aimed to acquire data on key soil properties. In particular, the fieldwork aimed to identify the texture and infiltration rate of the three non-rock land covers. At a total of 16 sites, a soil sample of ~500 g derived from the uppermost 50 cm of the soil was obtained for textural analysis. Each soil sample was sieved to separate the soil particles by size to enable specification of the relevant SCS soil group (Skaggs and Khaleel, 1982; SCS, 1986). The infiltration rate of each class was also assessed. Using a ring infiltrometer, inserted to a depth of 15 cm, the rate of infiltration was assessed with the change in measured vertical infiltration as a function of time used to derive an estimate of the infiltration rate (Philip, 1957); the nature of the surface cover across the test site ensured that splash effects could be ignored. Together, the information on soil texture and infiltration were used to determine the soil group for each class.

With the digital elevation model and curve numbers derived with the aid of the soil and land cover data, the HMS model was run. For this, the CRWR-PrePro system was used to calculate the required model parameters for each sub-basin. CRWR-PrePro was driven with the digital elevation, stream network and curve number data derived with the stream velocity and Muskingham × parameters set at 3 ms^{-1}, typical of that observed in arid regions (Allam and Balkhair, 1987; Reid et al., 1998), and 0.2, respectively. From these inputs, CRWR-PrePro was used to derive the average curve number and lag time as well as the longest flow path and its average slope for each sub-basin. The output from the HMS model was the flood hydrograph for outlet of the entire basin or each defined sub-basin. As concern here was on the potential of flood damage to the Idfu-Marsa-Alam road, the point where a sub-basin intersected the road was treated as an outlet and the hydrograph derived for that location. Of the 55 sub-basins that the road crossed 30 were very small, <1 km^2, and so excluded from further analyses as the potential for flood damage was consequently small. For the remaining 25 sub-basins the hydrograph was modelled and attention focused on the magnitude of the hydrograph's peak value as this is linked to the destructive force of the flood waters.

4. Results and discussion

Although, the three soil types exhibited different textures (Fig. 5) their textural description did not differ significantly in terms of the US Soil Conservation Service's (SCS, 1986) soil group classification. From the textural description derived, all three soils appeared to belong to soil group A, being coarse textured with little silt and clay and so having a low run-off potential. Field based observation of infiltration, however, indicated some important differences between the classes that could be used to refine the soil group allocations. In particular, the field studies revealed that the defined land cover classes differed in terms of key hydrological properties. Field measurements of infiltration rate at the site, for example, ranged from 0.07 cm h^{-1} on the desert pavement through 9.70 and 14.01 cm h^{-1} for the consolidated and unconsolidated wadi bed deposits, respectively.

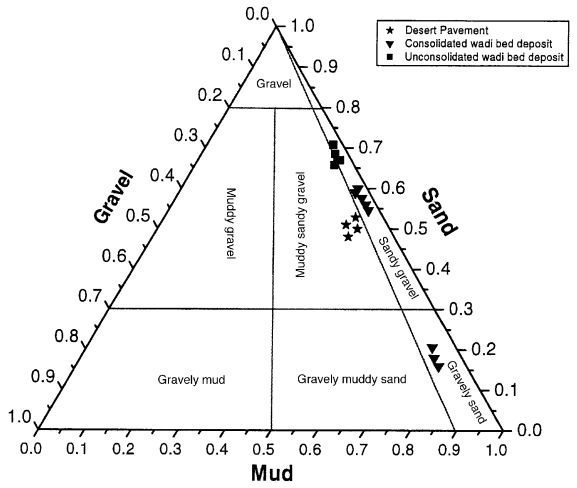

Fig. 5. Summary of the soil textural description derived from fieldwork.

The differences between these land covers in terms of infiltration is shown in Fig. 6. These measured soil infiltration rates supported the allocation of wadi bed deposits to group A. However, the infiltration rates observed also indicated that the desert pavement response was more similar to a soil in group D, with a high run-off potential. On the basis of the infiltration rate data, therefore, the wadi bed deposits were allocated to soil group A and the desert pavement to soil group D. These soil group allocations, together with the land cover data derived from the Landsat TM data, were used to specify the curve number for use in the HMS model.

The accuracy of the land cover map derived by the image classification was estimated to be 89.5% (Table 1), above the commonly specified target accuracy (85%) for many thematic maps (Foody, 2002). This representation of the land cover of the site was considered to be sufficiently accurate for use in driving the hydrological model. The model was run over the entire wadi basin as well as for the selected sub-basins that had an outlet intersecting the Idfu-Marsa-Alam road.

For each of the 25 sub-basin outlets that lay along the road between Marsa-Alam and Idfu, a hydrograph was derived from the HMS model. For this, a rainfall event with an intensity of 30 mm h^{-1} over a period of 2 h was assumed. This value lies within the range of storms observed in the general region (e.g. Gheith and Sultan, 2002) and was observed for the nearby Quseir station of the Egyptian Meteorological Authority on 14 November 1996. It was also assumed that the rainstorm uniformly and exclusively covered a specified single basin on each run of the model.

The peak discharge derived from each of the 25 sub-basins intersecting the road varied from 1.47 to 142.12 $m^3 s^{-1}$ (Fig. 7). As the peak discharge is positively related to the potential for flood damage it is apparent that the flood hazard varies significantly along the road. Additionally, a small number of sites were associated with particularly large peak discharges (Fig. 8). The two sites along the road known to have suffered significant flood damage in the recent past (El-Etr and Ashmawy, 1993) corresponded to the sites estimated to have the two highest peak discharges, located at approximately 13.5 and 29.0 km along the road from the edge of

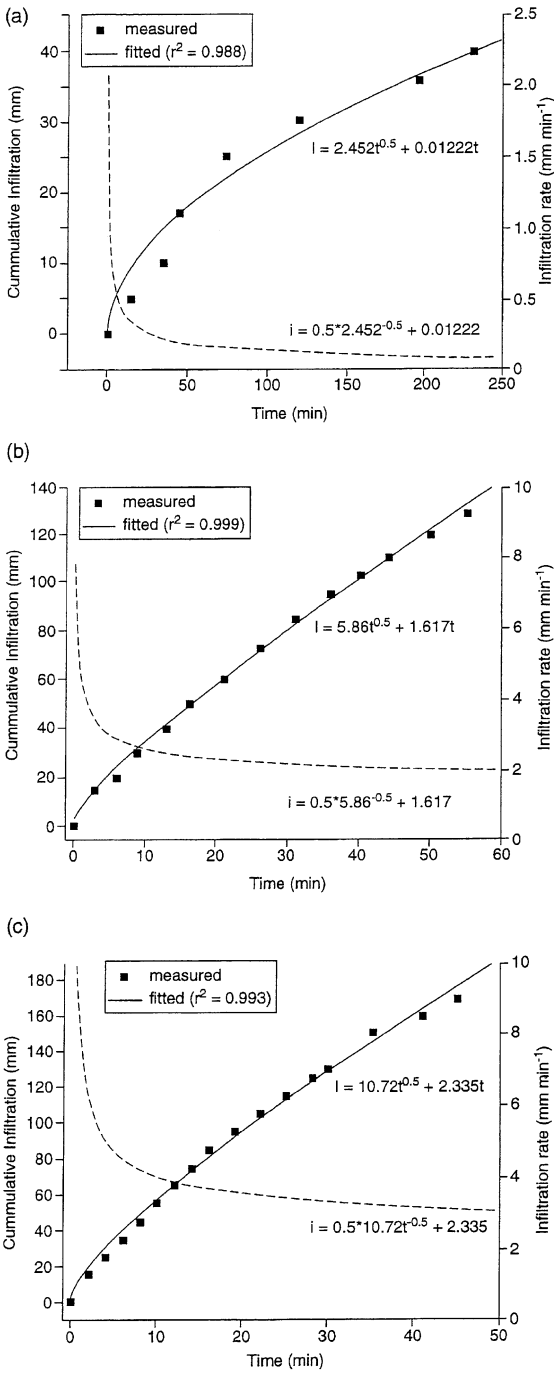

Fig. 6. Infiltration properties of the non-rock land covers (a) desert pavement, (b) consolidated wadi bed deposit, and (c) unconsolidated wadi bed deposit. In each graph the term I indicates the cumulative infiltration measured (left hand axis) and i the infiltration rate (right hand axis).

Table 1
Confusion matrix for land cover classification accuracy assessment

	C	U	S	D	B	Total	Producer's accuracy
Consolidated wadi bed deposit (C)	**43**	1	0	3	1	48	89.6
Unconsolidated wadi bed deposit (U)	2	**19**	0	0	0	21	90.5
Sedimentary rocks (S)	0	2	**17**	0	1	20	85.0
Desert pavement (D)	3	0	0	**44**	3	50	88.0
Basement rocks (B)	3	0	0	5	**82**	90	91.1
Total	51	22	17	52	87	229	
User's accuracy	84.3	86.4	100.0	84.6	94.3		

Note the rows represent the actual class of membership and the columns the predicted class of membership. Elements highlighted in bold represent correct class allocations. The overall percentage of cases correctly classified was 89.5% with the accuracy of each class >84% from both the map user's and producer's perspectives.

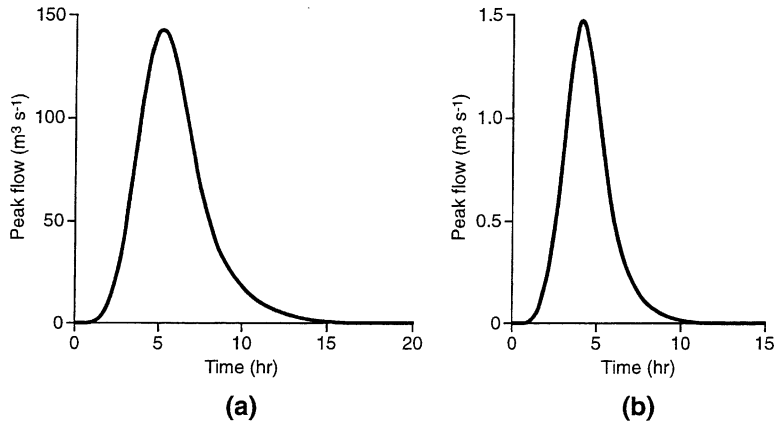

Fig. 7. Hydrographs indicating the range of discharges predicted. Note the 100 fold difference in the discharges represented.

the catchment boundary (Fig. 8) confirming the hazard vulnerability inferred from the modelling.

Flooding hazards at the site are not constrained to the Idfu-Marsa-Alam road, the major Red Sea coastal highway, for example, runs close to the Red sea shore crossing the El-Alam alluvial fan (Fig. 1) and so is subject to flooding from the wadi basin as a whole. Damage to this road may, however, be limited as the road was constructed close to the wadi floor and so, after a flood event, it is often simply covered in sediment that is easy to remove. The pedestrian surface beside the road was, however, constructed ~1 m above the wadi floor level and even though protected by large culverts, parts were washed away when the culverts were plugged with coarse deposits in a flood event in 1996 (Fig. 9). Finally, the flood hazard also affects the settlement of Marsa-Alam itself. Marsa-Alam is expanding, in particular growing along the wadi El-Alam. In places, attempts have

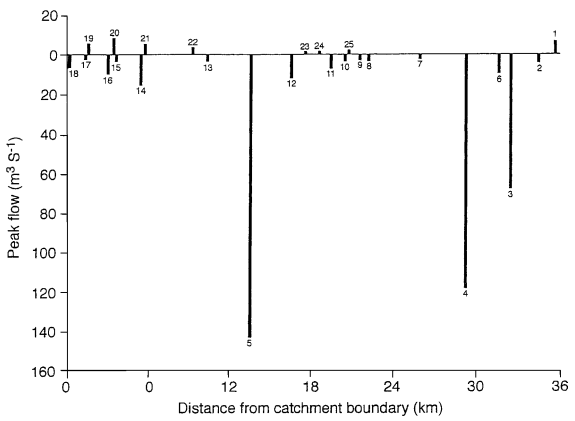

Fig. 8. Predicted peak flows from the 25 sub-basins. Numbered labels relate to the sub-basin identifiers shown in Fig. 1. For presentational reasons the horizontal line represents the road so that the flows from basins draining from the north (above the line) and south (below the line) may be discriminated. Note the two extremely large peak flows predicted that correspond with the locations damaged by recent floods.

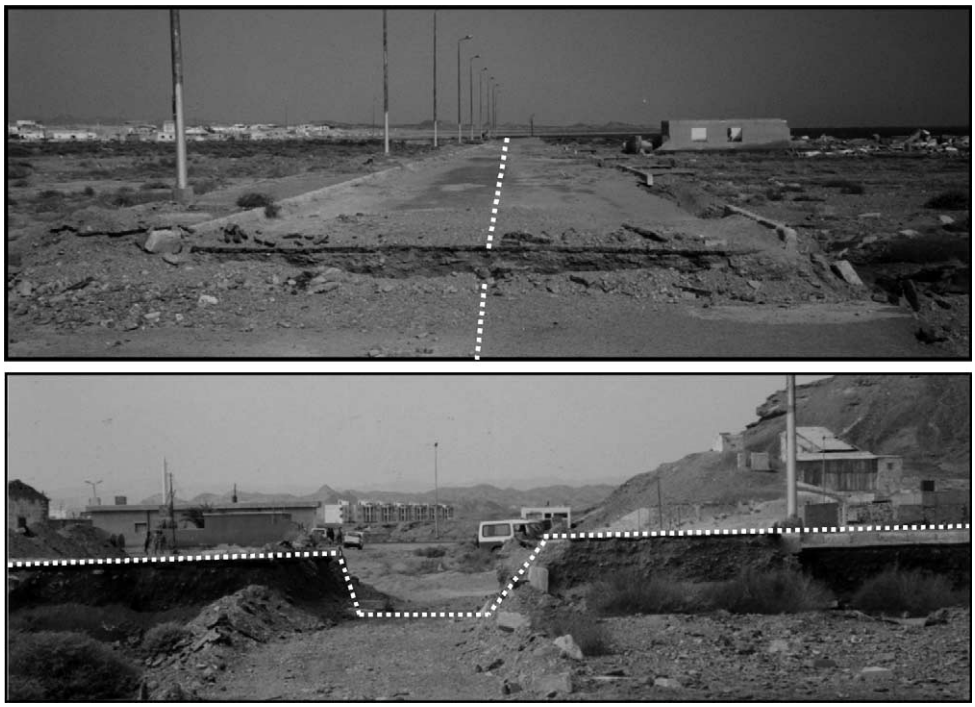

Fig. 9. Part of the pedestrian walkway damaged by a flood in 1996. The line annotated runs along the length of the walkway and shows the general vertical profile after the flood damage in the bottom image.

been made to minimise potential flood damage by building on the top of sediment rock hills but these locations may still be sensitive to lateral erosion from flood water and so may still be at risk from hazards associated with flash flood events.

5. Summary and conclusion

Flooding hazards in arid environments are well known but poorly understood due to a lack of data. Consequently, many infrastructure developments such as roads are poorly located and protected from flood hazards. This paper has demonstrated that the location of sites particularly at risk from large peak flows associated with flash flooding may be predicted using a hydrological model in which key parameters were derived from conventional topographic maps, field survey and a land cover map derived from satellite remote sensing.

Acknowledgements

We are grateful to the Egyptian Government for funding EMG's research studentship for a PhD degree at the University of Southampton and to the two referees for their constructive comments on the article.

References

Allam, M.N., Balkhair, S.K., 1987. Case study evaluation of the geomorphic instantaneous unit hydrograph. Water Resources Management 1, 267–291.

Baker, V.R., Benito, G., Rudoy, A.N., 1993. Paleohydrology of late pleistocene superflooding, Altay mountains, Siberia. Science 258, 348–350.

Bishop, M.P., Colby, J.D., 2002. Anisotropic reflectance correction of SPOT-3 HRV imagery. International Journal of Remote Sensing 23, 2125–2131.

Chavez, P.S., 1996. Image-based atmospheric corrections—revised and revisited. Photogrammetric Engineering and Remote Sensing 62, 1025–1036.

Chlebek, A., Jarabac, M., 2002. In: Snorasson, A., Finnsdottir, H.P., Moss, M. (Eds.), The Extremes of the Extremes: Extraordinary Floods, IAHS Publication 271, International Association of Hydrological Sciences, Wallingford, pp. 19–23.

Chow, V.T., Maidment, D.R., Mays, L.W., 1988. Applied Hydrology. McGraw-Hill, New York.

Colby, J.D., Keating, P.L., 1998. Land cover classification using Landsat TM imagery in the tropical highlands: the influence of anisitropic reflectance. International Journal of Remote Sensing 19, 1479–1500.

Douglas, I., Bidin, K., Balamurugan, G., Chappell, N.A., Walsh, R.P.D., Greer, T., Sinun, W., 1999. The role of extreme events in the impacts of selective tropical forestry on erosion during harvesting and recovery phases at Danum Valley, Sabah. Philosophical Transactions of the Royal Society B 354, 1749–1761.

Ekstrand, S., 1996. Landsat TM-based forest damage assessment: correction for topographic effects. Photogrammetric Engineering and Remote Sensing 62, 151–161.

El-Etr, H., Ashmawy, M., 1993. Flash flood vulnerability and mitigation of the Red Sea basins between latitudes 24°41′ and 25°26′, Egypt. In: Proceedings of the International Conference 30 Years Cooper, Geological Survey of Egypt, Cairo, pp. 335–361.

Engman, E.T., Gurney, R.J., 1991. Remote Sensing in Hydrology. Chapman and Hall, London.

Foody, G.M., 2002. Status of land cover classification accuracy assessment. Remote Sensing of Environment 80, 185–201.

Foody, G.M., 2004. Mapping land cover from remotely sensed imagery for input to hydrological models. In: Abrahart, R.J., See, L., Kneale, P.E. (Eds.), Neural Networks for Hydrological Modelling, Swets and Zeitlinger, Lisse, 269–289.

Gheith, H., Sultan, M., 2002. Construction of a hydrologic model for estimating Wadi runoff and groundwater recharge in the Eastern Desert, Egypt. Journal of Hydrology 263, 36–55.

Graef, F., Haigis, J., 2001. Spatial and temporal rainfall variability in the Sahel and its effects on farmers management strategies. Journal of Arid Environments 48, 221–231.

Greenbaum, N., Margalit, A., Schick, A.B., Backer, V.R., 1998. A high magnitude storm and flood in a hyperarid catchment, Nahal Zin, Negev Desert, Israel. Hydrological Processes 12, 1–23.

Herschy, R., 2002. The world's maximum observed floods. In: Snorasson, A., Finnsdottir, H.P., Moss, M. (Eds.), The Extremes of the Extremes: Extraordinary Floods, 271. IAHS Publication 271, International Association of Hydrological Sciences, Wallington, pp. 355–360.

Hoshi, T., Uchida, S., Kotoda, K., 1989. Development of a system to estimate evapotranspiration over complex terrain using Landsat MSS, elevation and meteorological data. Hydrological Sciences Journal 4, 635–649.

Langley, S.K., Cheshire, H.M., Humes, K.S., 2001. A comparison of single date and multitemporal satellite image classifications in a semi-arid grassland. Journal of Arid Environments 49, 401–411.

Mather, P.M., 1999. Computer Processing of Remotely-Sensed Images, second ed., Wiley, Chichester.

Mimikou, M., Baltas, E., Varanou, E., 2002. A study of extreme storm events in the Greater Athens area, Greece. In: Snorasson, A., Finnsdottir, H.P., Moss, M. (Eds.), The Extremes of the Extremes: Extraordinary Floods, IAHS Publication 271, International Association of Hydrological Sciences, Wallingford, pp. 161–165.

Oba, G., 2001. The effect of multiple droughts on cattle in Obbu, Northern Kenya. Journal of Arid Environments 49, 375–386.

Olivera, F., Maidment, D.R., 1999. GIS tools for HMS modelling support. In: Maidment, D.R., Djokic, D. (Eds.), Hydrologic and Hydraulic Modelling Support, ESRI Press, Redlands, CA.

Papp, F., 2002. Extremes of extreme floods. In: Snorasson, A., Finnsdottir, H.P., Moss, M. (Eds.), The Extremes of the Extremes: Extraordinary Floods, IAHS Publication 271, International Association of Hydrologic Sciences, Davis, CA, pp. 373–378.

Peters, J.C., 1998. HEC-HMS, Hydrologic Modeling Systems, US Army Corps of Engineers, Hydrologic Engineering Center, Davis, CA.

Philip, J.R., 1957. The theory of infiltration: 4. Sorptivity and algebraic infiltration equations. Soil Science 84, 257–264.

Reid, I., Laronne, J.B., Powell, M.D., 1998. Flash-flood and bedload dynamics of desert gravel-bed streams. Hydrological Processes 12, 543–557.

Sabol, G.V., Stevens, K.A., 1990. Comparison of design criteria for the Southwest. In: French, R.H., (Ed.), Hydraulics/Hydrology of Arid Lands (H^2AL), American Society of Civil Engineers, New York, pp. 102–107.

SCS, 1985. National Engineering Handbook, US Department of Agriculture, Soil Conservation Service, Washington, DC.

SCS, 1986. Urban Hydrology for Small Watersheds, Technical Release 55, US Department of Agriculture, Soil Conservation Service, Sprinfield VA.

Sharma, K.D., Singh, S., 1992. Runoff estimation using Landsat Thematic Mapper data and the SCS model. Hydrological Sciences Journal 37, 39–52.

Skaggs, R.W., Khaleel, R., 1982. Infiltration, Hydrologic Modelling of Small Watersheds. American Society of Agricultural Engineers, St Joseph, MI.

Song, C., Woodcock, C.E., Set, K.C., Pax-Lenney, M., Macomber, S.A., 2001. Classification and change detection using Landsat TM data: when and how to correct atmospheric effects. Remote Sensing of Environment 75, 230–244.

Storck, P., Bowling, L., Wetherbee, P., Lettenmaier, D., 1998. Application of a GIS-based distributed hydrology model for prediction of forest harvest effects on peak stream flow in the Pacific Northwest. Hydrological Processes 12, 889–904.

Su, Z., 2000. Remote sensing of land use and vegetation for mesoscale hydrological studies. International Journal of Remote Sensing 21, 213–233.

Tso, B., Mather, P.M., 2001. Classification Methods for Remotely Sensed Data. Taylor and Francis, London.

Zeller, M.E., 1990. Precipitation on arid and semi-arid regions in the southwestern United States: research needs from a consultant's perspective. In: French, R.H., (Ed.), Hydraulics/Hydrology of Arid Lands (H^2AL), American Society of Civil Engineers, New York, pp. 525–529.